Real Time Phase Shifting with an Adjustable Inertance Tube

W.J. Zhou and J.M. Pfotenhauer

Cryogenics Laboratory, University of Wisconsin - Madison
Madison, WI, USA 53706

ABSTRACT

As a follow up to previous exploratory measurements, we report on the phase shifting characteristics of an adjustable inertance tube coupled to a pulse tube refrigerator. The phase difference between mass flow and pressure oscillations at the inlet of the adjustable inertance tube is measured using calibrated pressure and mass flow transducers and a Labview-based lock-in amplifier. The mass flow signal is obtained from the pressure drop across a screen pack, suitably designed by balancing the competing requirements of a sufficiently large signal size and minimal acoustic power loss. By using the distributed component model, the phase between the mass flow and pressure wave are compared with the experiment. A large acoustic power flow, up to 1500 W is measured when the cryocooler runs at 42 Hz. Although there are minor discrepancies between the measured and calculated phase angle, the trend of its dependence on the length of the inertance tube fits well with the model prediction.

INTRODUCTION

A long narrow tube was first adopted by Kanao [1] in 1994 to produce a phase shift in a pulse tube cryocooler. Since then, this component has been used extensively to fix the phase between the pressure and flow oscillations in high frequency pulse tube cryocoolers. Zhu [2] reported that the long neck tube can obviously improve the performance of the pulse tube cryocooler, because it can generate a larger phase shift than either the orifice or double inlet configurations. Gardner [3] introduced a lumped component model to describe the complex impedance inside the inertance tube.

Roach [4] used a simplified electrical analogy to show the advantages of using a long neck tube in the design of pulse tube cryocoolers, and was the first to name the component an 'inertance tube.' de Boer [5] applied a simple turbulent flow model to the inertance tube and found that the performance of the pulse tube with an inertance tube is superior to that of the orifice pulse tube cryocooler. Luo *et al.*[6] developed a laminar-flow thermoacoustic transmission-line model and a turbulent-flow thermoacoustic model to describe the performance of the inertance tube. Lewis *et al.*[7,8] considered the impedance match between the pulse tube and the inertance tube and measured the phase shift of a variety of inertance tubes. Schunk *et al.*[9] developed a distributed component model to characterize the complex impedance of the inertance tube. The contour plots from their paper display the phase shift and acoustic power as they depend on the dimensions of the inertance tube; these can guide the design of inertance tubes for desired phase shift and acoustic power. Radebaugh *et al.*[10] used the transmission line model to optimize the diameter and length
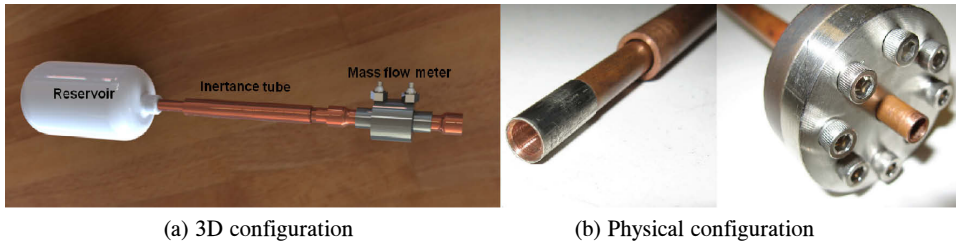
(a) 3D configuration   (b) Physical configuration

Figure 1. Structure of variable inertance tube

of the inertance tube. The transmission line model data fit the experimental results very well. Lewis *et al.*[11] measured the impedance of the inertance tube for frequencies up to 150 Hz. Pfotenhauer *et al.*[12] reported an innovated method to utilize the length dependence of the phase shift by using an adjustable inertance tube. The performance of high frequency pulse tube cryocoolers largely depends on the phase shift between the mass flow and pressure oscillations. Use of the inertance tube can force the mass flow to either lead or lag the pressure; therefore, it is helpful to study how the length and diameter of the inertance tube affect the performance of the cryocooler.

Although it is clear that setting the proper inertance tube dimensions can optimize the performance of pulse tube cryocoolers, it is also clear that changing the dimensions of inertance tubes — especially during pulse tube operation — is a difficult challenge. In this paper, we report further data gathered with the adjustable length inertance tube described in Pfotenhauer *et al.* [11]. In the present report, a relatively thin screen pack is used for the mass flow measurement, thereby avoiding a large drop in acoustic power across that screen pack. The resulting phase shifts produced by the inertance tube were therefore not limited by a low value of acoustic power in that device. Pictures of the variable inertance tube are shown in Figure 1. The mass flow and pressure at the inlet of the inertance tube are measured using a 6-piece copper screen pack (80 mesh), and two pressure sensors, one on each side of the screen pack. With these devices, the mass flow, pressure, and phase shift between pressure and mass flow at the inlet of the inertance tube are measured and discussed in details in the following paragraphs.

MATHEMATICAL MODEL

There are several models that can describe the mechanism in the inertance tube. The lumped component model was first introduced by Gardener *et al*[3]; it models the inertance tube as a single complex impedance within the pulse tube cryocooler. Due to its simplicity, the lumped component model is widely used to qualitatively calculate the impedance of the inertance tube. Luo *et al.* [6] developed a transmission line model in which several ODEs with complex variables are solved analytically for the laminar flow case, and numerically in the turbulent flow case. The distributed component model developed by Schunk *et al.* [9] provides an advantage over the transmission line model if the number of nodes in the model is very large. The distributed component model can account for variations in the mass flow along the length of the tube, but more significantly at the entrance and exit of the tube. In Schunk's paper, the distributed component model fit the experimental data very well; however, he was unable to compare the experimental results with the expected mass flow and acoustic power at the warm end of the pulse tube due to limitations in the achieved measurements. In the present investigation, the screen pack enables a direct measurement of the mass flow, acoustic power, and phase shift at the warm end of the pulse tube; this allows a comparison with the theoretical predictions for those quantities.

The distributed component model separately computes the inertance, resistance, and compliance values for the reservoir and for the n sections of the inertance tube. Figure 2 presents a schematic diagram of this model. The inertance tube is modeled as a large number of equi-length segments, each of which have associated complex impedance values for the fluid resistance ZiR, compliance ZiC, and inertance ZiL.
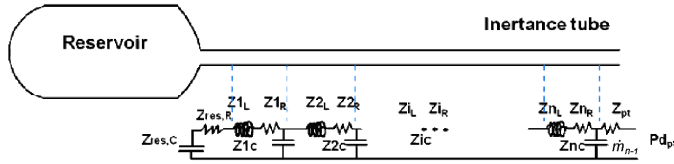
Figure 2. Schematic diagram of the distributed component model of the inertance and reservoir

For node number i, the fluid resistance Z_{iR} is:

$$Z_{i,R} = \frac{2.944 \, \text{Re}_i^{-0.2} \, \dot{m}_i \Delta L}{\pi^3 \rho_{he} D_{in}^5}$$ (1)

Here Re_i is the Reynolds number for each segment, which can be represented as:

$$\text{Re}_i = \dot{m}_i \frac{8}{\left(\pi^2 \cdot D_{in} \cdot \mu \right)}$$ (2)

μ is the viscosity of the helium gas in the inertance tube, and $\dot{m}_i$ is the amplitude of the mass flow rate of each section. $\Delta L = L/n$, ρ_{he} is the average density of helium gas inside inertance tube, and D_{in} is the inner diameter of the inertance tube. The inertance impedance, Z_{iL}, for the 'i'th node is:

$$Z_{i,L} = j\omega \frac{4\Delta L}{\pi D_{in}^2}$$ (3)

where j is the square root of negative one, and ω is the angular frequency.
The compliance for the 'i'th node can be represented as:

$$Z_{i,C} = \frac{1}{j\omega} \left(\frac{\pi D_{in}^2 \Delta L}{4\gamma R_g T} \right)^{-1}$$ (4)

where γ is the heat capacity ratio, R_g is the gas constant, and T is the average temperature in the tube. Beginning with the reservoir as displayed in Figure 2, and summing up the impedance terms for each node (going left to right), the impedance at the first node in the inertance tube is obtained by a series addition:

$$Z_{1,s} = Z_{res,c} + Z_{res,R} + Z_{1,L} + Z_{1,R}$$ (5)

The compliance impedance, being in parallel with the term from Eq. 5 is added as:

$$Z_{1,p} = \left(\frac{1}{Z_{1,s}} + \frac{1}{Z_{1,C}} \right)^{-1}$$ (6)

The subsequent series- and parallel- added impedance terms (from node 2 to n) are determined by:

$$Z_{i,s} = Z_{i-1,p} + Z_{i,R} + Z_{i,L} \quad and \quad Z_{i,p} = \left(\frac{1}{Z_{i,s}} + \frac{1}{Z_{i,C}} \right)^{-1}$$ (7)

So that the total impedance of the entire network can be written as:

$$Z_{fin} = Z_{n,p} + Z_{e,R}$$ (8)

where $Z_{e,R}$ represent the flow resistance associated with an exit effect at the point where the inertance tube joins the pulse tube.

Table 1. Basic input parameters

P0 (pa)	2.07e6	Frequency (Hz)	50
Pd (pa)	2.28e5	T (K)	294
D_{in} (m)	4.83e-3	V_{res} (m^3)	1e-3
L (m)	1.529	n	10

The magnitude of the mass flow rate at the entrance of the inertance tube is

$$\dot{m}_{n+1} = \frac{Pd_{pt}}{Z_{fin}} \tag{9}$$

Pd_{pt} is the pressure amplitude at the inlet of the inertance tube. The acoustic power at this junction between the pulse tube and inertance tube is:

$$\dot{W}_{ac} = R_g T_h \frac{Pd_{pt}^2}{2 P_0 | Z_{fin} |} \cos(\theta_{pt,h}) \tag{10}$$

Here T_h is the temperature at the hot end of the pulse tube, P_0 is the average pressure in the pulse tube, and the phase angle between the mass flow and pressure oscillations is:

$$\theta_{pt} = -\angle Z_{fin} \tag{11}$$

Also, we define dimensionless length and dimensionless acoustic power as follows:

$$\bar{L} = \frac{L}{\lambda} \tag{12}$$

$$\bar{W}_{ac} = \frac{4 W_{ac}}{\pi D^2 P_0 a} \tag{13}$$

Where λ is the helium wave length, and 'a' is the velocity of sound in helium gas.

The inputs to the distributed component model are the average pressure P_0, the pressure amplitude Pd at the inlet of the inertance tube, the inner diameter D_{in} and length L of the inertance tube, and the frequency ω of the oscillations. Nominal values for these parameters, as used within the present report, are shown in Table 1 (L and frequency are varied). With these inputs and the known fluids properties, the mass flow, acoustic power, and also the phase shift at each node of the inertance tube can be easily calculated.

COMPARISON BETWEEN EXPERIMENTS AND THEORY

An experimental setup was carried out to measure the mass flow, phase shift and the acoustic power at the inlet of the inertance tube. The mass flow inside the inertance tube is measured by the mass flow device, which is shown in Figure 1(a). The mass flow meter is assembled by stacking six copper screens (80 meshes) in the space between the two flanges. Two pressure transducers are mounted at each end of the screen pack to measure the pressure drop through the mass flow meter.

The phase shift between the mass flow and pressure oscillations is detected by the Labview Lock-in amplifier program. The phase difference between the pressure oscillation on the pulse tube side of the screen pack and the mass flow through the screen pack are determined by the Lock-in vi (virtual instrument).

The acoustic power going through the inertance tube is deduced from the product of the pressure amplitude at the outlet of the pulse tube, the mass flow through the screen pack (divided by the gas density on the pulse tube side of the screen pack), and the phase angle detected by the Lock-in amplifier program.

The mass flow meter measures the pressure wave both before and after the screen pack. The pressure waves at the mass flow meter are shown in Figure 3. The average pressure in this example
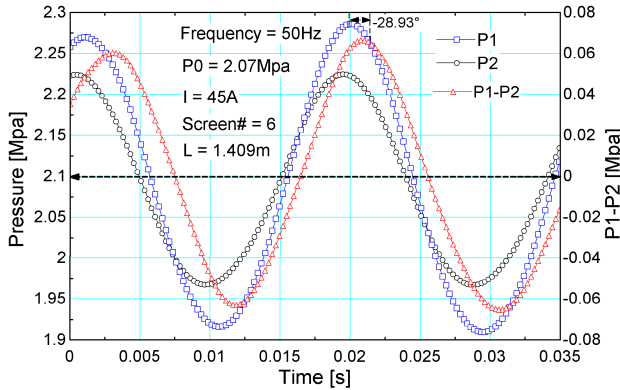
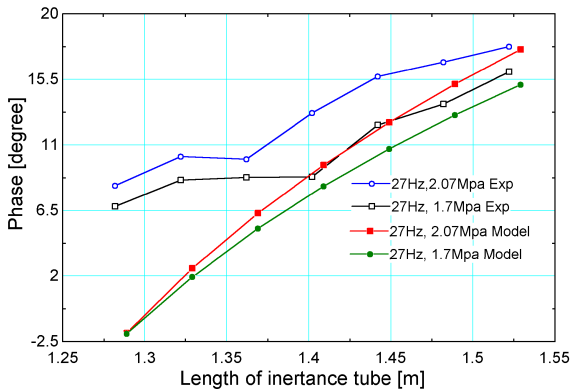**Figure 3.** Phase shift between mass flow and pressure

Figure 4. Phase shift change with length at 27 Hz

is 2.07 MPa, and the pressure amplitude at the warm end of the pulse tube Pd is about 0.205 MPa. Due to the nonzero flow impedance across the screen pack, the pressure amplitude at the inlet of the inertance tube is about 0.155 MPa. With this pressure difference, the Lock-in amplifier can easily obtain the phase shift between the mass flow and pressure wave at the warm end of the pulse tube. In the case shown in Figure 3, the operating frequency is 50 Hz and the length of the variable inertance tube is 1.409 m, so that a 28.93º phase shift is measured between the mass flow and pressure oscillations.

The influence of the inertance tube length on the phase shift between the mass flow and pressure oscillations at 27 Hz is shown in Figure 4 for two different average pressures, 2.07 MPa and 1.7 MPa. The phase angle changes from 7.5º to 18.5º as the length varies from 1.289 m to 1.529 m, a 15.6% change in length. As a comparison, the phase shift from the distributed component model is also shown here. A small, but noticeable discrepancy exists at the shorter length, but the curves converge as the length increases. Also, the change of phase over this length change is about 12º from the model compared to 11º from the experiment.

Additional experiments have been carried out by varying the frequency from 27 Hz to 50 Hz. The phase shifts as a function of inertance tube length at 42 Hz and 50 Hz are shown in Figure 5 and Figure 6, respectively. The phase angle shifts from 26.5º to 31.5º as the length changes from 1.289 m to 1.529 m at 42 Hz. Also, the same trend is predicted by the model. From Figure 6, there is only a 3.5º phase shift as the length of the inertance tube varies from 1.289 m to 1.529 m at 50 Hz. Although there are some discrepancies between the experimental data and model calculation, both display the same trends in Figure 5 and Figure 6. Various mechanisms such a tube roughness, heat
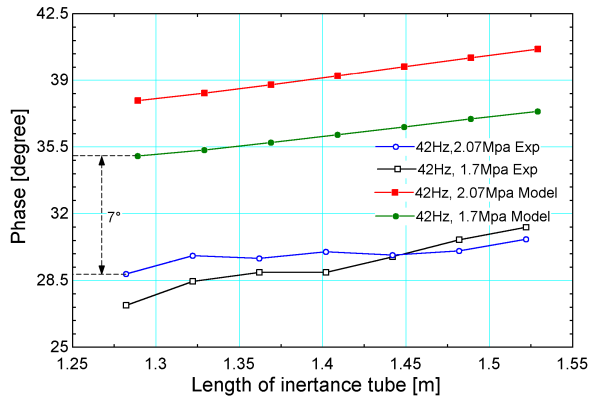
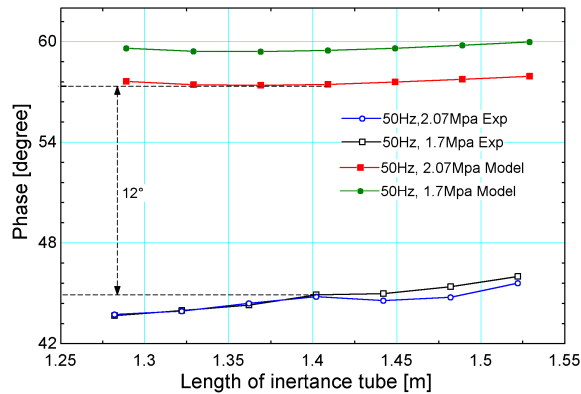**Figure 5.** Phase shift change with length at 42 Hz

Figure 6. Phase shift change with length at 50 Hz

transfer and exit/entrance effects are being explored to resolve the discrepancy. However, both the experiment and model reflect the same change of phase that can be affected by the change in inertance tube length. From the data presented in Figures 4, 5, and 6, one can conclude that the phase shift is more sensitive to changes in the inertance tube length at lower frequencies than at higher frequencies.

Phase angle changes as a function of frequency from 52 Hz to 27 Hz at average pressures of 2.07 MPa and 1.7 MPa are displayed in Figure 7 and Figure 8. The phase generally decreases from around -10º to around 45º as the operating frequency increases from 27 Hz to 52 Hz. Both the experimental data and model data reflect the same trend. Although the discrepancy between the model and measurements is minor at the lower frequencies, it increases as the frequency increases. Figures 7 and 8, also reflect a sensitive dependence of the phase shift on length at lower frequencies, such as 27 Hz, but a significantly reduced sensitivity at higher frequencies. A larger change in length is required in order to obtain a large phase shift if the cryocooler runs at a higher frequency.

Adjusting the length of the inertance tube not only varies the phase angle between the mass flow and pressure oscillations, but also the mass flow amplitude and the acoustic power at the warm end of pulse tube vary with length and operating frequency. Figure 9 displays the variation of mass flow amplitude with length at different frequencies. The trend of the measurements and model again are very similar. At 27 Hz, the model fits the experiment very well. However, at the higher frequencies, such as 42 Hz and 50 Hz, small discrepancies may be observed. The peak in the mass flow amplitude around 42 Hz is in keeping with expectations presented by Lou *et al.* [6].
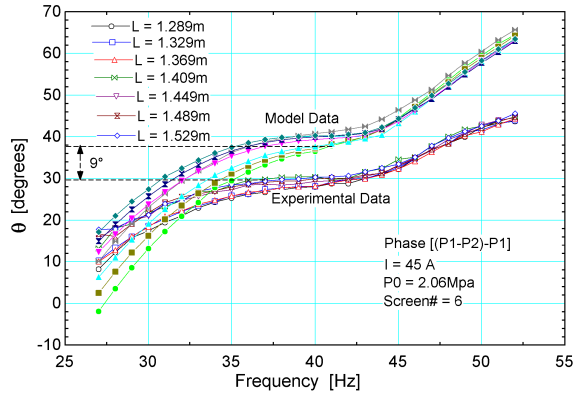
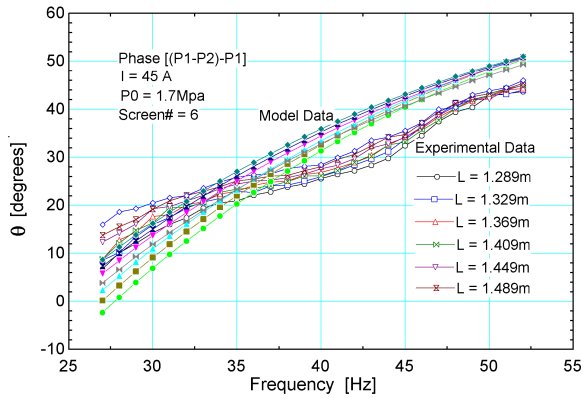**Figure 7.** Phase shift changes with frequency at 2.06 Mpa

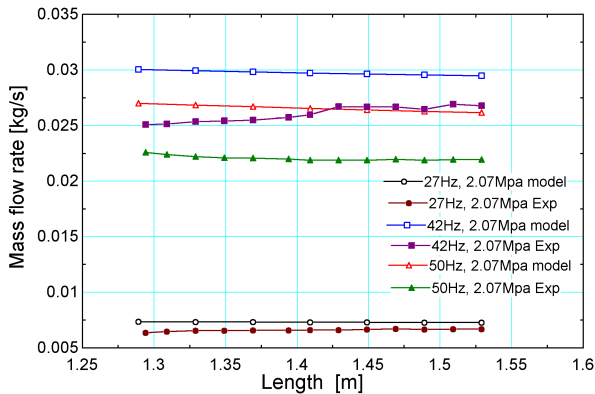**Figure 8.** Phase shift changes with frequency at 1.7 Mpa

Figure 9. Mass flow change with length

From the mass flow, pressure amplitude, and phase angle between these two parameters, the acoustic power is easily obtained via the simple acoustic power expression. The change in acoustic power with the length is shown in Figure 10. The acoustic power increases slightly from 141.6 W to 150 W as the length ranges from 1.289 m to 1.529 m at 27 Hz. These small changes are a result of the configuration limitations in our experiment. The largest percentage change to the inertance tube
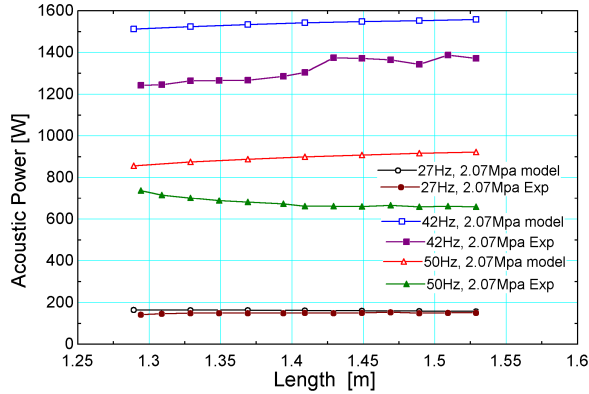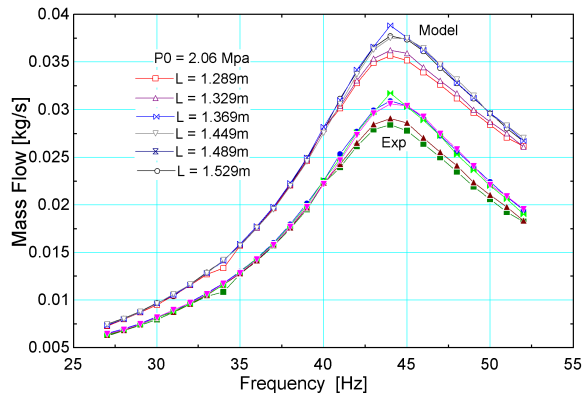
Figure 10. Acoustic power change with length

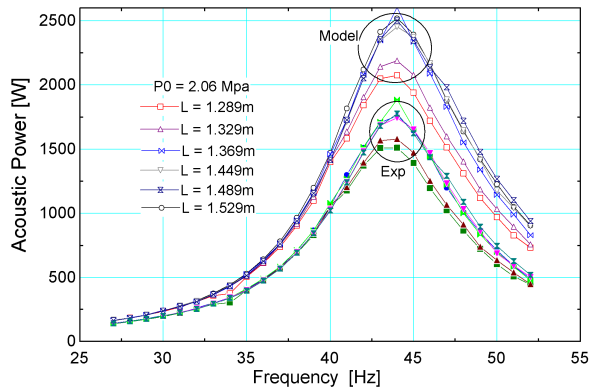
Figure 11. Mass flow change with frequency

Figure 12. Acoustic power change with frequency

length in our present configuration is limited to only 16% of total length. Future efforts will be directed at modifying and increasing the possible change of length.

Figure 11 and Figure 12 display the variations of mass flow amplitude and acoustic power as a function of the operating frequency and inertance tube length. For our inertance tube, a maximum in both the mass flow amplitude and acoustic power is observed around 42 Hz. Notice that a small
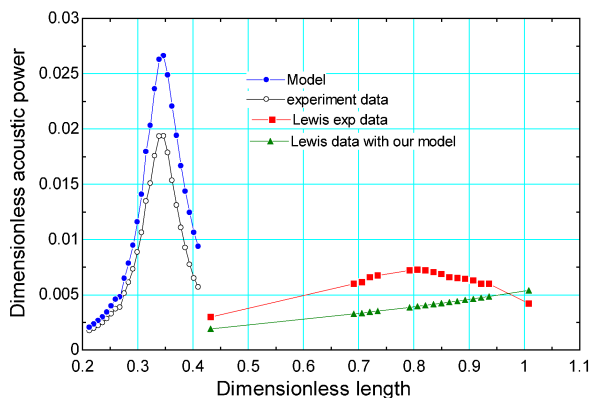
Figure 13. Comparison of the other paper's data

length change can generate a relatively large variation in the mass flow amplitude and acoustic power at this frequency. Both the measurements and the model display the same trends as a function of frequency and length.

In an effort to confirm the predictions of the model with other published data, we display in Figure 13 the data and modeling results for the single case of L= 1.289 m, D=4.83 mm, and P_0 = 2.06 MPa, along with that reported by Lewis et al.[8] for L = 2.36 m, D= 5.74 mm and P_0 = 2.5 MPa. Note that the distributed component model accurately predicts both sets of data. Furthermore, the peaking behavior evident in both sets of data correlates well with the predictions of Luo et al. In Figure 3 of Luo et al. a maximum in the acoustic power is found near the dimensionless lengths of 0.35 and 0.8 (allowing for large, but finite sized reservoirs), with the larger peak at the dimensionless length of 0.35. At 42 Hz our dimensionless length is 0.33 while at 57 Hz, the dimensionless length associated with the data presented by Lewis et al. is 0.82.

DISCUSSION AND CONCLUSIONS

By using a screen-pack mass flow meter and an adjustable inertance tube, measurements have been obtained that describe changes in the phase shift, mass flow amplitude, and acoustic power resultant from variations in inertance tube length and operating frequency. The observed trends match the predictions of the distributed component model. The mass flow and pressure oscillations, as well as the phase difference between them at the inlet of the inertance tube are measured from the experiment, and these match the model predictions. At lower frequencies, such as 27 Hz, the phase shift is very sensitive to the length changes of the inertance tubes. A maximum is observed in the mass flow amplitude and acoustic power around 42 Hz, also in agreement with the model.

A few relatively small discrepancies exist between the model and experiments. Future efforts, both in the application of the model and in experimental configurations will be pursued. In addition to expanding the percentage range of length variations, future experiments will also be directed at variable inertance tube diameters.

REFERENCES

1. Kanao, K.-i., N. Watanabe, and Y. Kanazawa, "A miniature pulse tube refrigerator for temperatures below 100K," *Cryogenics*, 34 (1994)**,** pp. 167-170.

2. Zhu S, et al., "Phase shift effect of the long neck tube for the pulse tube refrigerator," *Cryocoolers 9*, Plenum Press, New York (1997), pp. 269-278.

3. Gardner, D.L. and G.W. Swift, "Use of inertance in orifice pulse tube refrigerators," *Cryogenics*, 37:2 (1997), pp. 117-121.

4. Roach, P.R. and Kashani, A., "Pulse tube coolers with an inertance tube: Theory, modeling, and prac-tice," *Adv. in Cryogenic Engineering*, 43, Kluwer Academic/Plenum Publishers, New York (1998), pp. 1895-1902.

5. de Boer, P.C.T., "Performance of the inertance pulse tube," *Cryogenics*, 42:3-4 (2002), pp. 209-221.

6. Luo, E., R. Radebaugh, and M. Lewis, "Inertance Tube Models and Their Experimental Verification," *Adv. in Cryogenic Engineering*, Vol. 49B, Amer. Institute of Physics, Melville, NY (2004), pp. 1485-1492.

7. Lewis, M.A., et al., "Measurements of Phase Shifts in an Inertance Tube," *Cryocoolers 13*, Springer Science+Business Media, New York (2005), pp. 267-273.

8. Lewis, M., Bradely, P.E., Radebaugh, R. Gan, Z.H., "Characterization of inertance tubes using reso-nance effects," *Cryocoolers 14*, ICC Press, Boulder, CO (2007), pp. 263-270.

9. Schunk, L.O., Nellis, G.F. and Pfotenhauer, J.M., "Experimental Investigation and Modeling of Iner-tance Tubes," *Journal of Fluids Engineering*, 127:5 (2005), pp. 1029-1037.

10. Radebaugh, R., et al., "Inertance Tube Optimization for Pulse Tube Refrigerators," *Adv. in Cryogenic Engineering*, Vol. 51, Amer. Institute of Physics, Melville, NY (2006), pp. 59-67.

11. Lewis, M.A., et al., "Impedance Measurements of Inertance Tubes at High Frequency and Pressure," *Adv. in Cryogenic Engineering*, Vol. 53, Amer. Institute of Physics, Melville, NY (2008), pp. 1083-1090.

12. Pfotenhauer, J. M., Steiner, T. and Qiu, L.M., "Continuously Variable Inertance Tubes for Pulse Tube Refrigerators," *Cryocoolers 16*, ICC Press, Boulder, CO (2011), pp. 275-280.